Electronic Supplementary Material (ESI) for Soft Matter.

Supplementary Figures for Microscopic origin of tunable assembly forces in chiral active environments

Clay H. Batton and Grant M. Rotskoff*
Department of Chemistry, Stanford University, Stanford, CA, USA 94305
(Dated: May 2, 2024)

Appendix A: Supplementary Figures

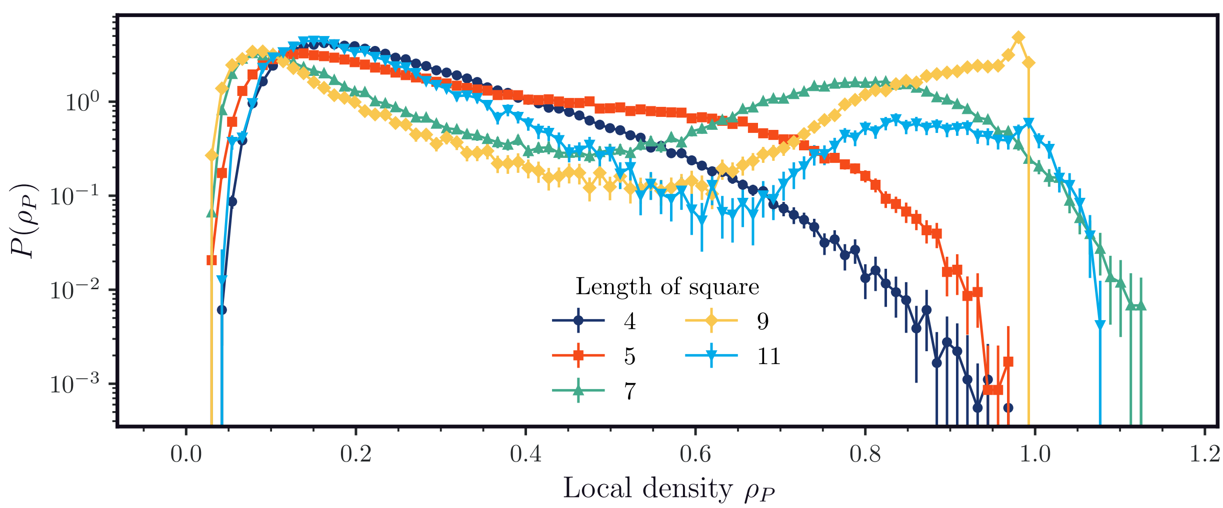

FIG. S1: Histograms of the local density of passive square particles of varying length for $\phi_A = 0.2$, $\phi_P = 0.2$, $\nu = 80$, and $\omega = 5$.

* rotskoff@stanford.edu

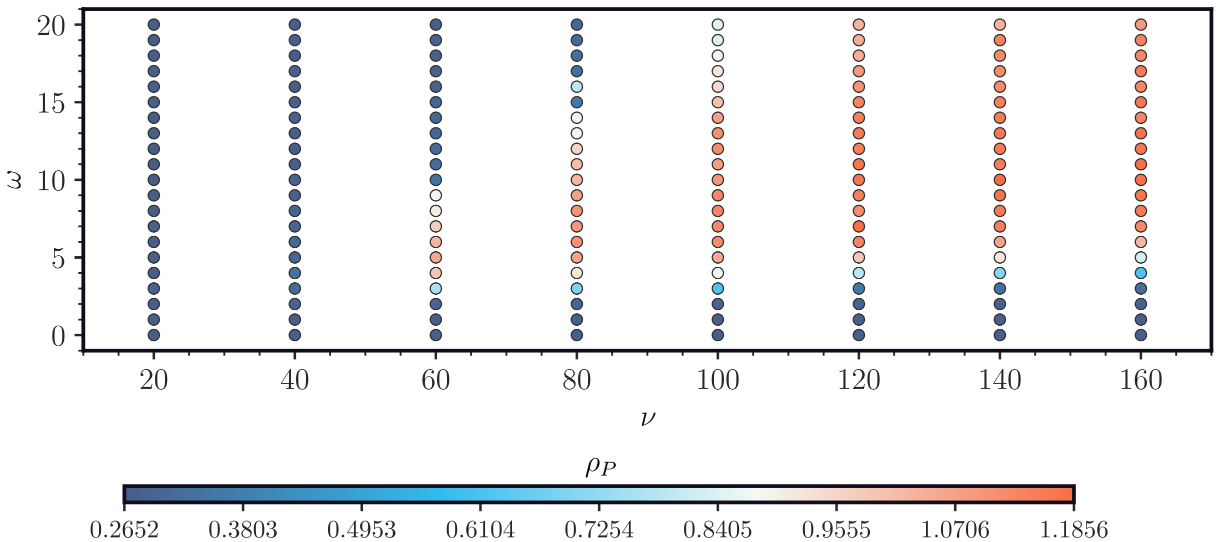

FIG. S2: Average density of passive square particles in the cluster phase for varying ν and ω for $\phi_A = 0.2$, $\phi_P = 0.2$, and $L = 9\ \sigma$. In cases where the system remains homogeneous, the cluster density is set equal to the overall passive particle density.

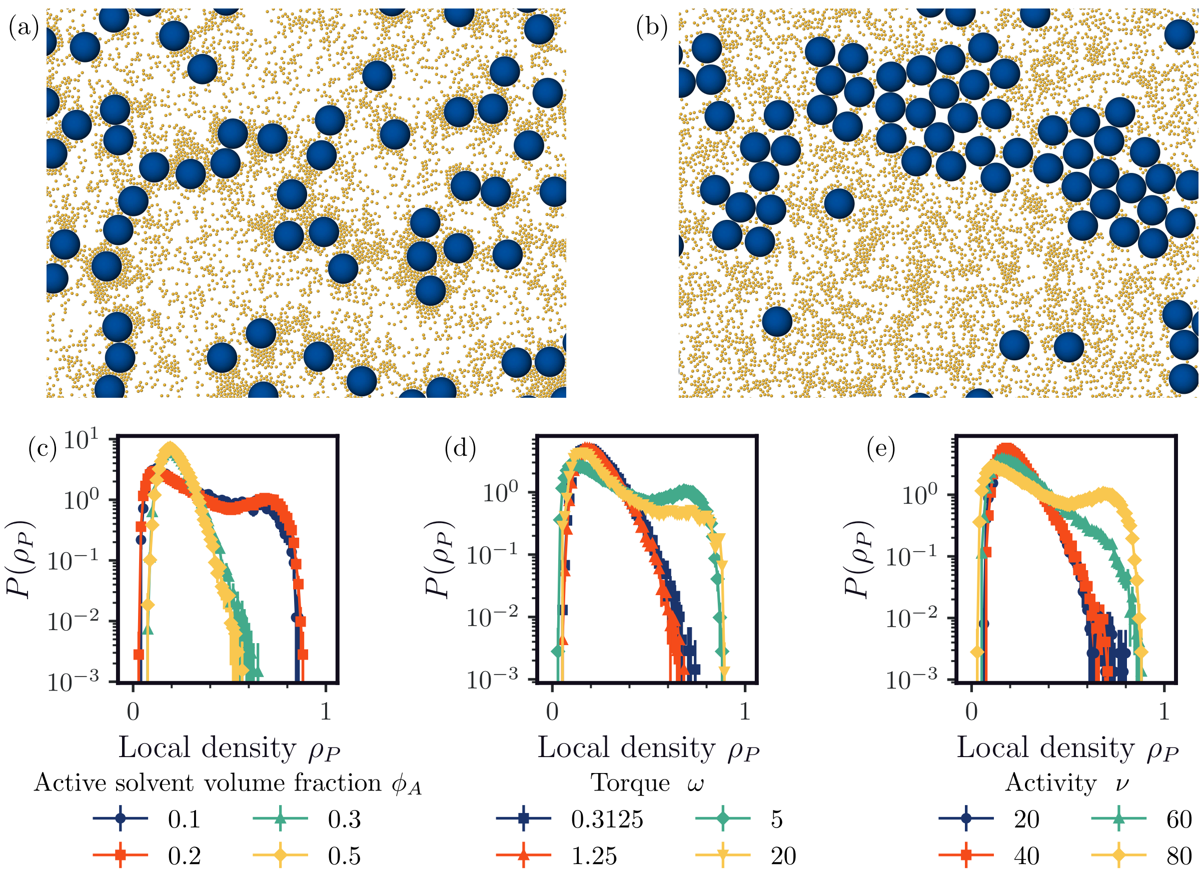

FIG. S3: Multiple passive disks of radii 5 σ in a chiral active Brownian particle bath with a passive volume fraction of 0.2. (a,b) Systems where the passive disks do not and do assemble for $\phi_A = 0.2$, $\nu = 80$, and (a) $\omega = 0.3125$ and (b) $\omega = 5$, respectively. Histograms of local density of the passive particles, ρ_P, for (c) varying ϕ_A at $\omega = 5$ and $\nu = 80$, (d) varying ω at $\phi_A = 0.2$ and $\nu = 80$, (e) varying ν at $\omega = 5$ and $\phi_A = 0.2$.

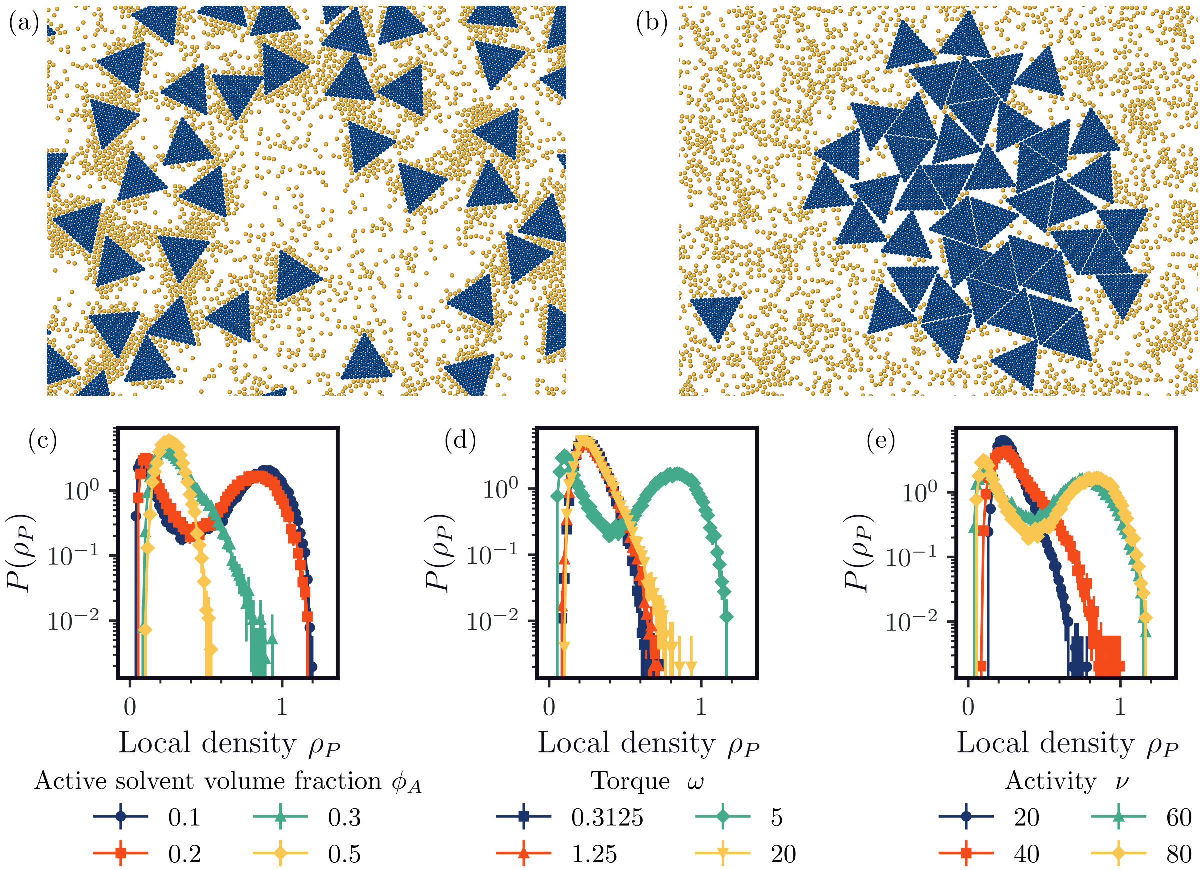

FIG. S4: Multiple passive triangles of side length 12 σ in a chiral active Brownian particle bath with a passive volume fraction of 0.2. (a,b) Systems where the passive triangles do not and do assemble for $\phi_A = 0.2$, $\nu = 80$, and (a) $\omega = 0.3125$ and (b) $\omega = 5$, respectively. Histograms of local density of the passive particles, ρ_P, for (c) varying ϕ_A at $\omega = 5$ and $\nu = 80$, (d) varying ω at $\phi_A = 0.2$ and $\nu = 80$, (e) varying ν at $\omega = 5$ and $\phi_A = 0.2$.

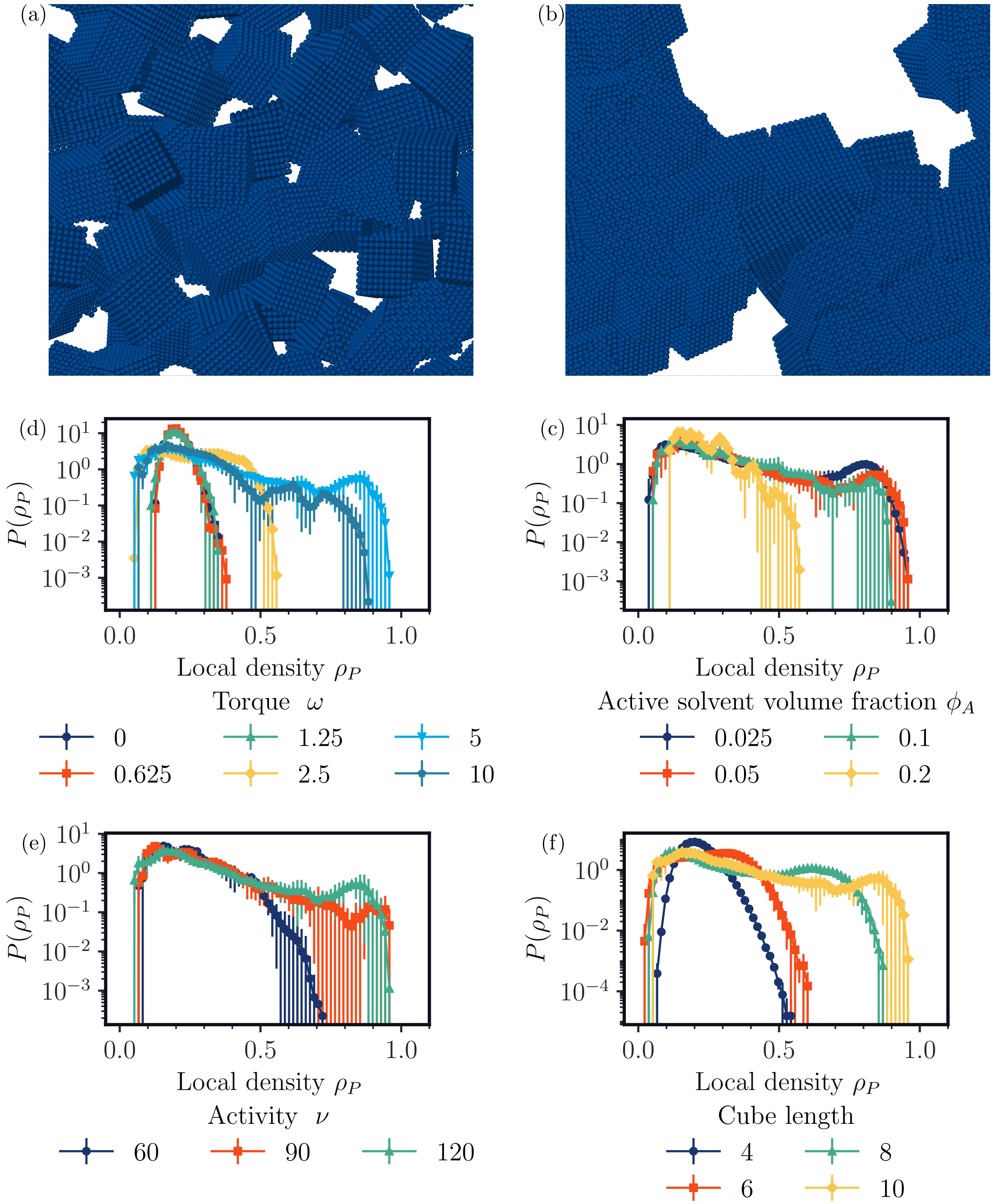

FIG. S5: Multiple passive cubes of length 10 σ in a chiral active Brownian particle bath with a passive volume fraction of 0.2 in three dimensions. (a,b) Systems where the passive cubes do not and do assemble for $\phi_A = 0.2$, $\nu = 120$, and (a) $\omega = 0.625$ and (b) $\omega = 5$, respectively, where the solvent is not visualized. Histograms of local density of the passive cube particles, ρ_P, for $\phi_P = 0.2$ at (c) varying ω with $\phi_A = 0.05$, $\nu = 120$ and $L = 10$ σ, (d) varying ϕ_A at $\nu = 120$, $\omega = 5$, and $L = 10$ σ, (e) varying ν at $\phi_A = 0.05$, $\omega = 5$, and $L = 10$ σ, (f) varying L at $\phi_A = 0.05$, $\nu = 120$, and $\omega = 5$.

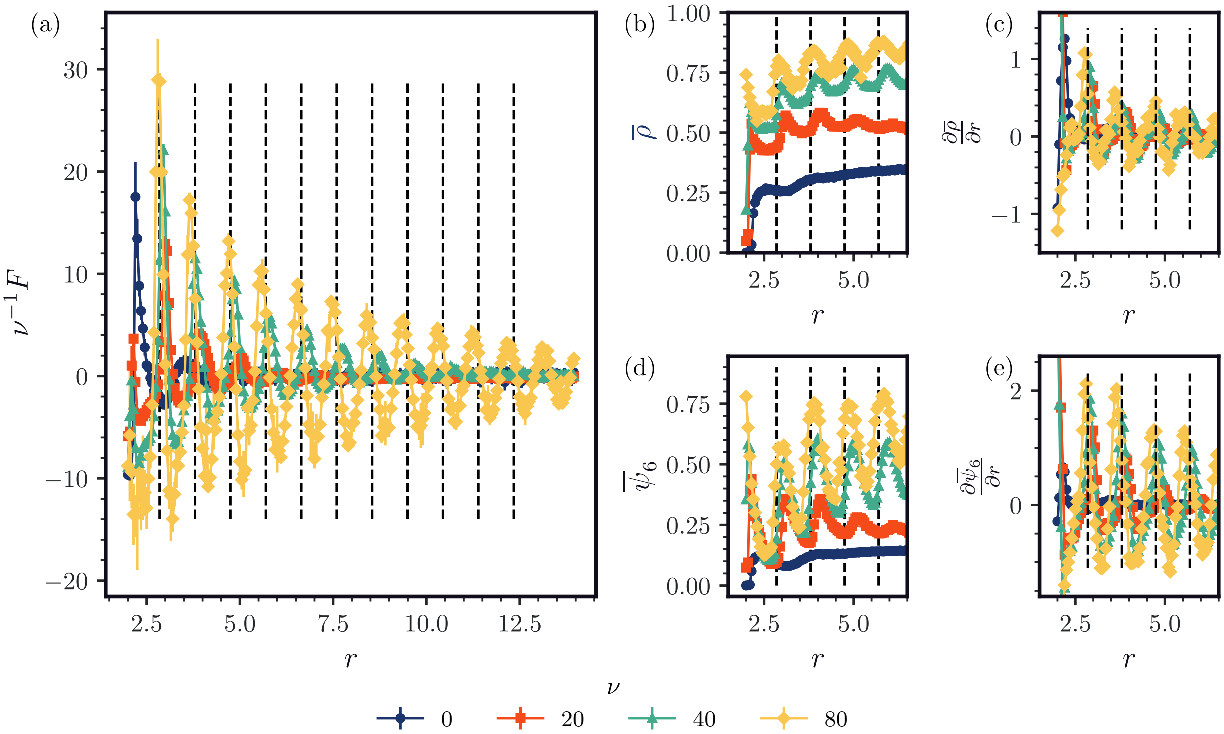

FIG. S6: Quantities obtained for a system with two passive walls of length 10 and $\rho = 0.4$ for varying ν and separation length. (a) Force F. (b) Density between walls, $\overline{\rho}$. (c) Hexatic order parameter between walls, $\frac{\partial\overline{\rho}}{\partial r}$. (d) $\overline{\psi}_6$. (e) $\frac{\partial\overline{\psi}_6}{\partial r}$. See Sec. C5 for further details on how the density and hexatic order parameter are computed.

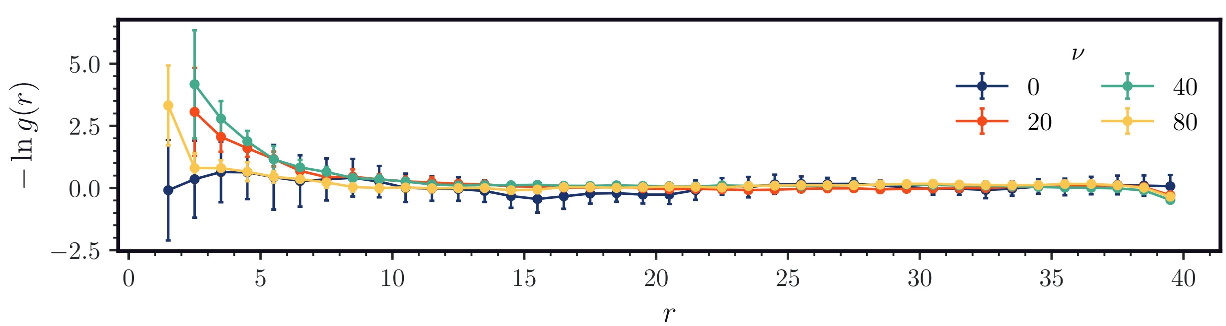

FIG. S7: The effective free energy $-\ln g(r)$ between two passive walls of length 10 and $\rho = 0.4$ for varying activity.

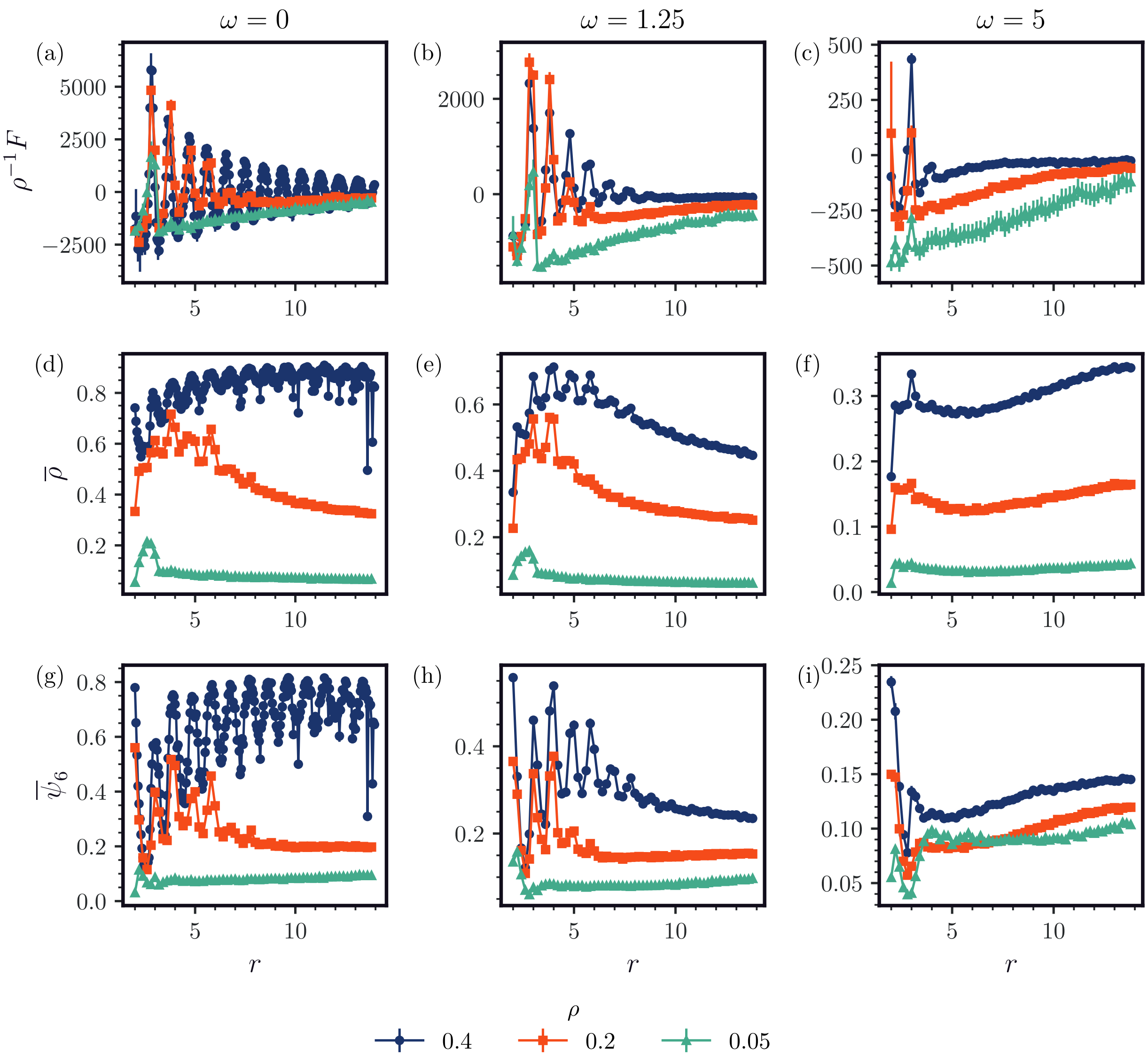

FIG. S8: $\rho^{-1}F$, $\overline{\rho}$, and $\overline{\psi}_6$ between two passive walls of length 10 for varying separation lengths, torque, and ρ for $\nu = 80$. See Sec. C5 for further details on how the density and hexatic order parameter are computed.

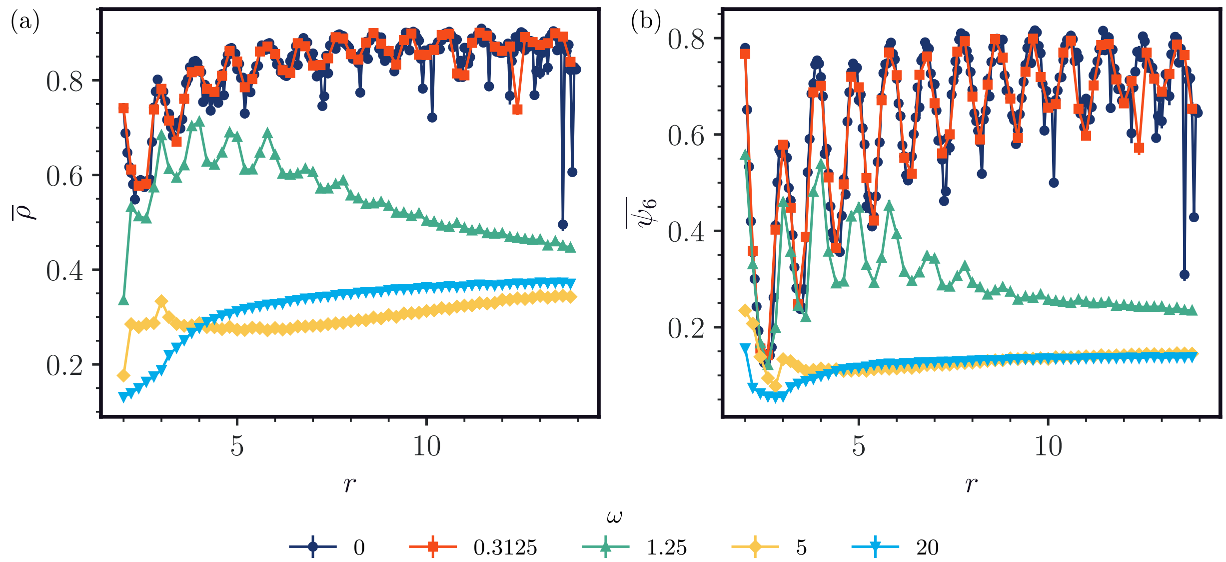

FIG. S9: (a) Average density $\overline{\rho}$ and (b) hexatic order parameter $\overline{\psi}_6$ between two passive walls of length 10, bulk $\rho = 0.4$, and $\nu = 80$ for varying torque and separation length. See Sec. C5 for further details on how the density and hexatic order parameter are computed.

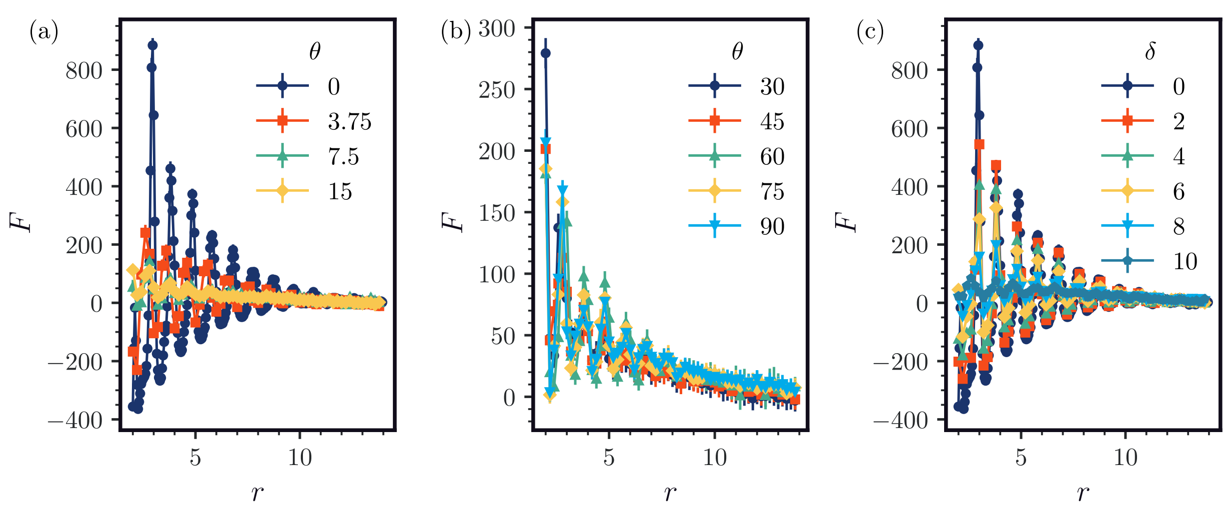

FIG. S10: Force between two passive walls of length 10, $\rho = 0.4$, and $\nu = 40$ for (a,b) varying angles θ between the walls and (c) varying offset δ between the walls.

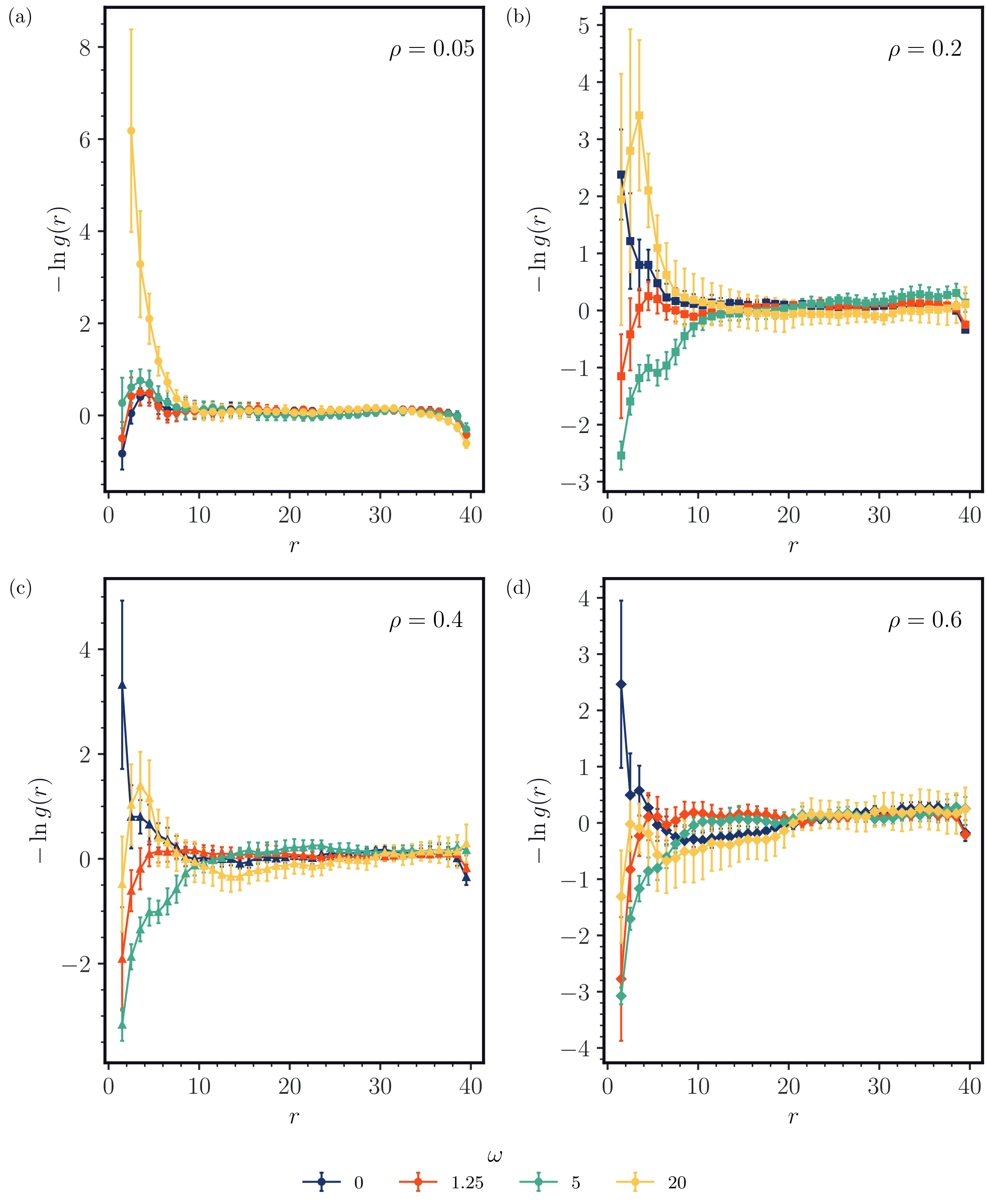

FIG. S11: Effective free energy between two passive walls of length 10 and $\nu = 80$ for varying ρ and ω.

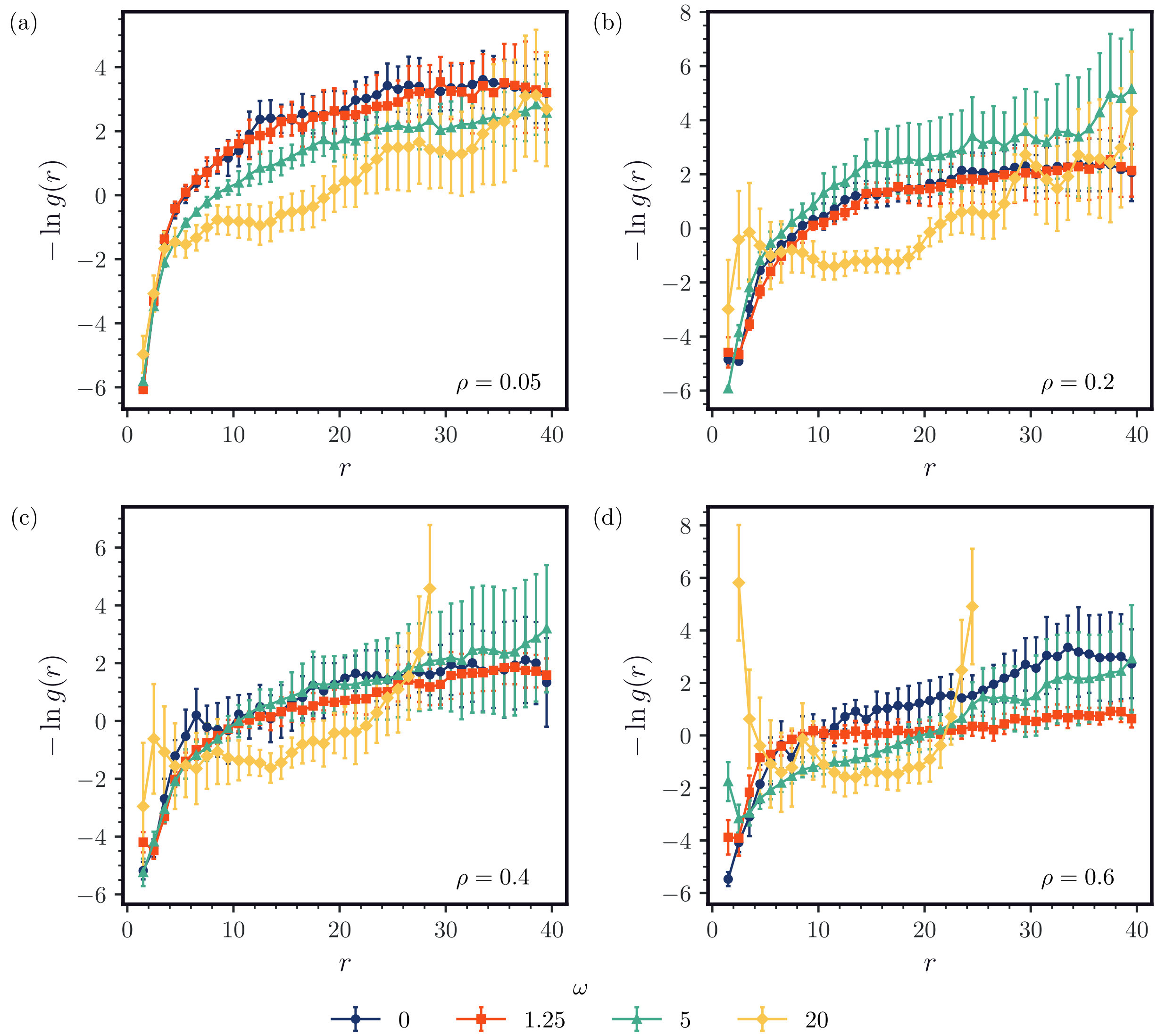

FIG. S12: Effective free energy between two passive walls of length 10 and $\nu = 80$ for varying ρ and ω that are constrained to move only in the x-direction and to not rotate. See Sec. C6 for further details on how the constraint is implemented.

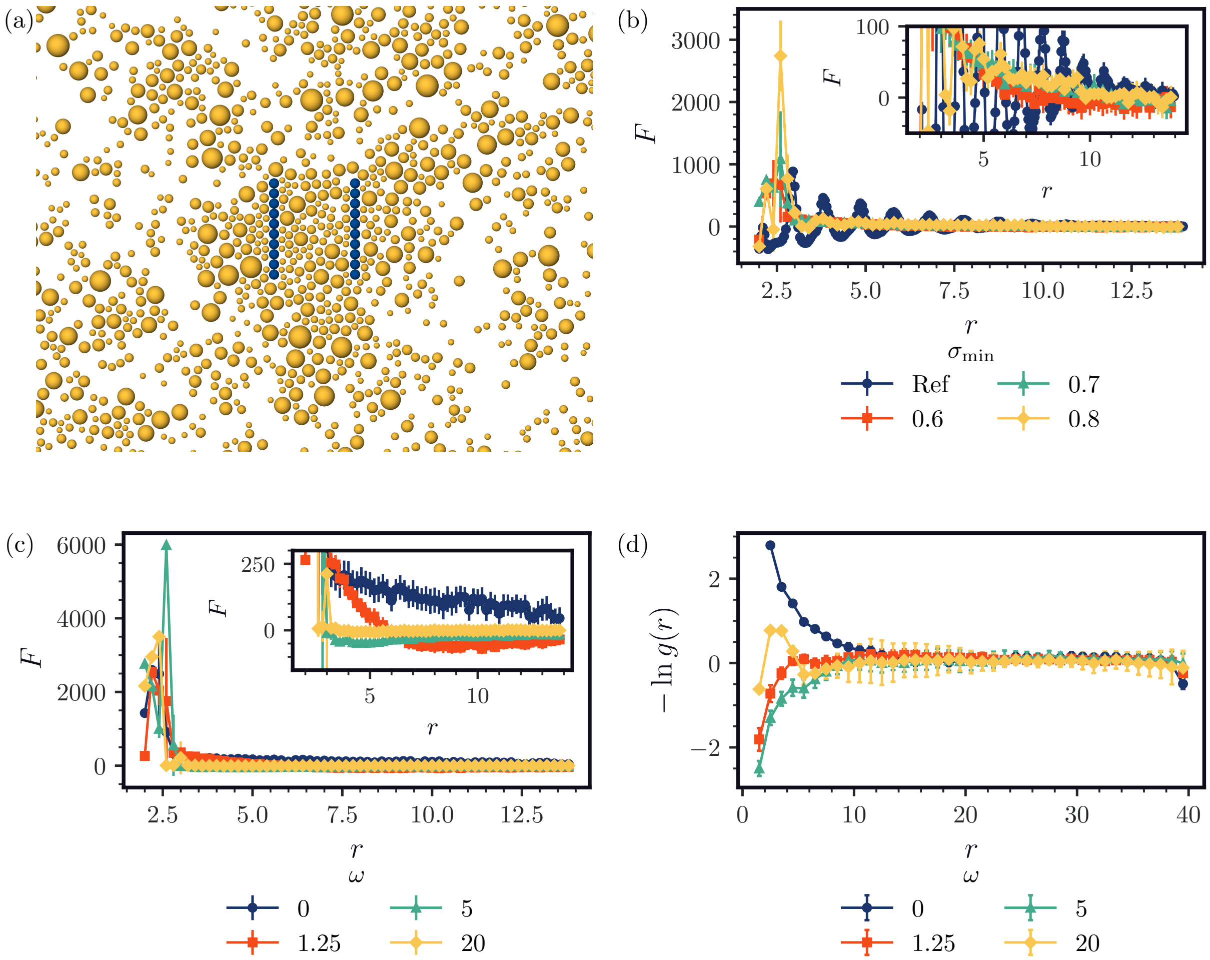

FIG. S13: Passive walls in a polydisperse active Brownian particle bath system. (a) Image of the system with $\rho = 0.4$, $\nu = 40$, and $\sigma_{\min} = 0.6$. (b) Force between two passive walls of length 10, $\rho = 0.4$, $\nu = 40$, and $\omega = 0$ for varying separation lengths and $\sigma_{\min}$. (c) Force and (d) $-\ln g(r)$ between two passive walls of length 10, $\rho = 0.4$, $\nu = 80$, and $\sigma_{\min} = 0.6$ for varying separation lengths and ω.

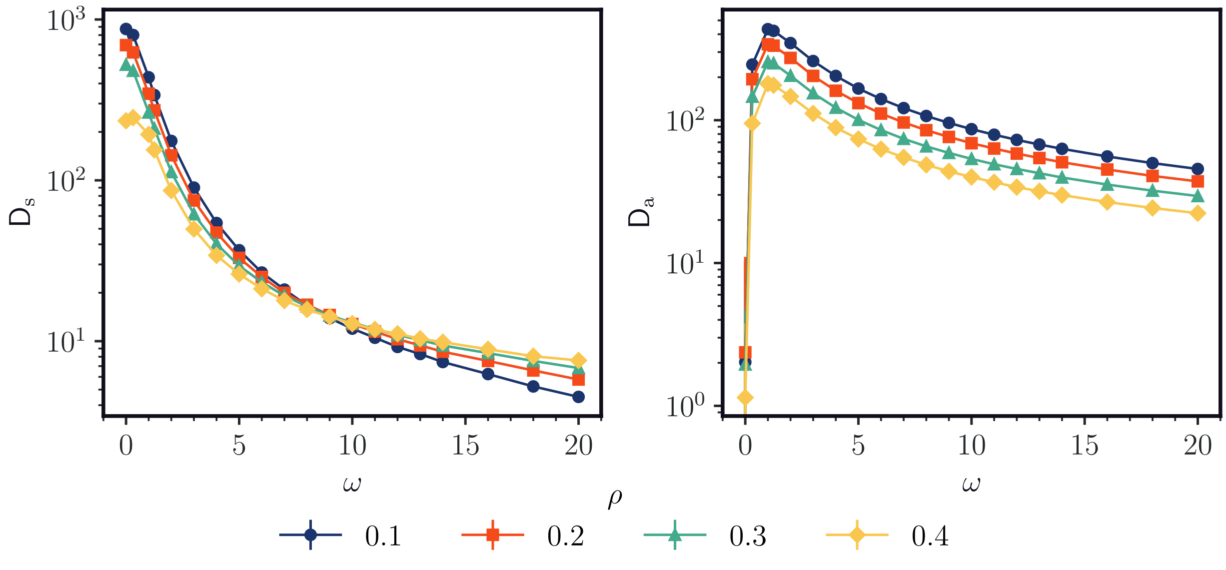

FIG. S14: Diffusion constants for varying ω and ρ at $\nu = 80$.

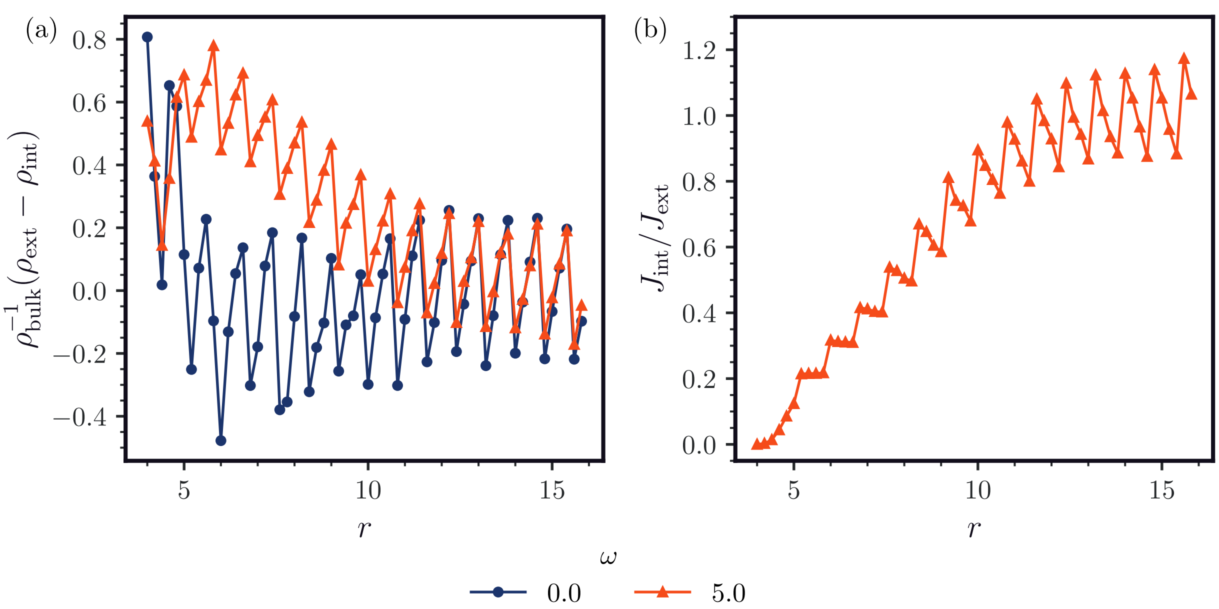

FIG. S15: (a) Difference between external and internal densities and (b) ratio of internal and external fluxes near the walls for varying ω at $\nu = 80$ and $\rho = 0.2$.

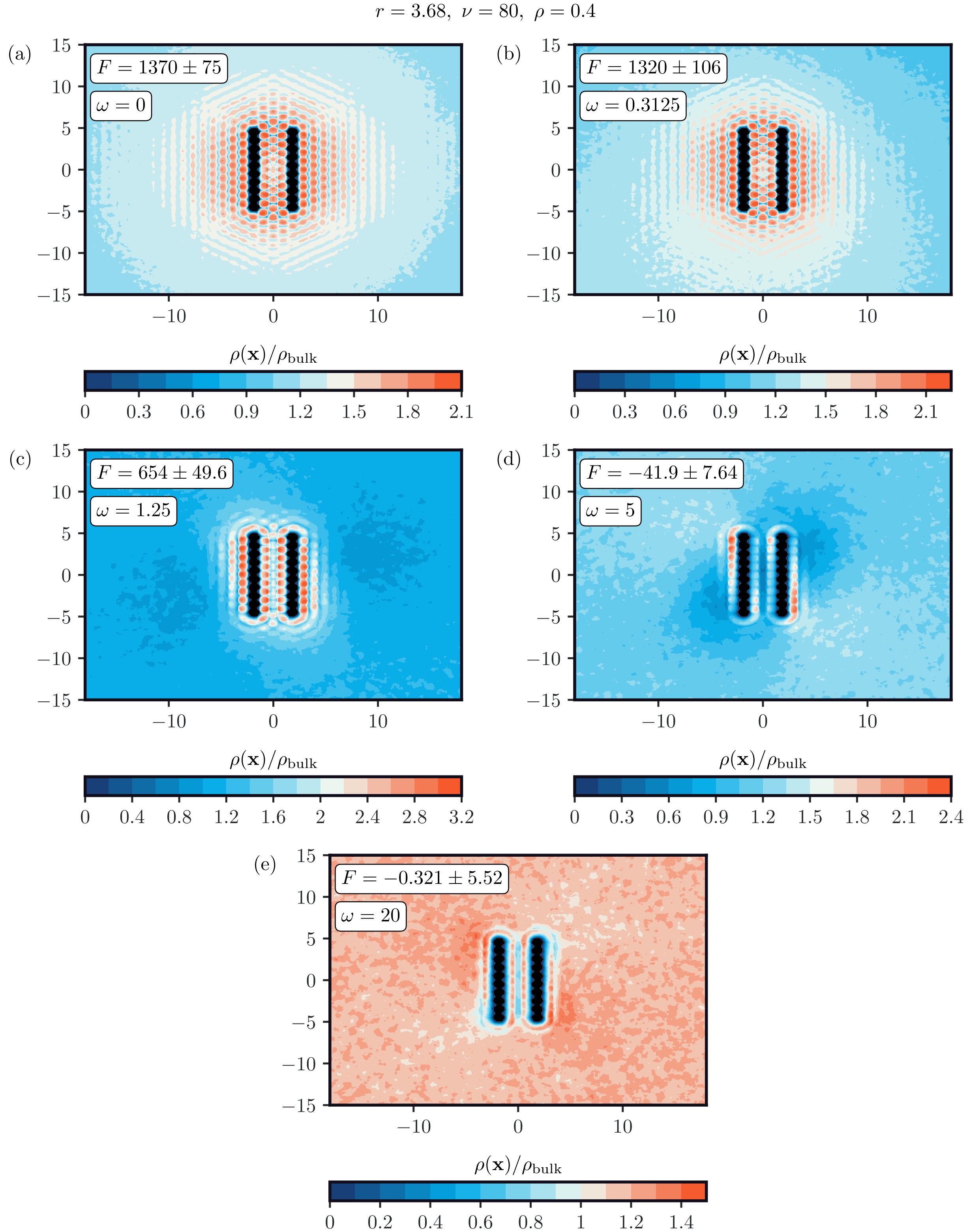

FIG. S16: Density fields for maximal repulsive force between two passive walls in a chiral active Brownian particle bath.

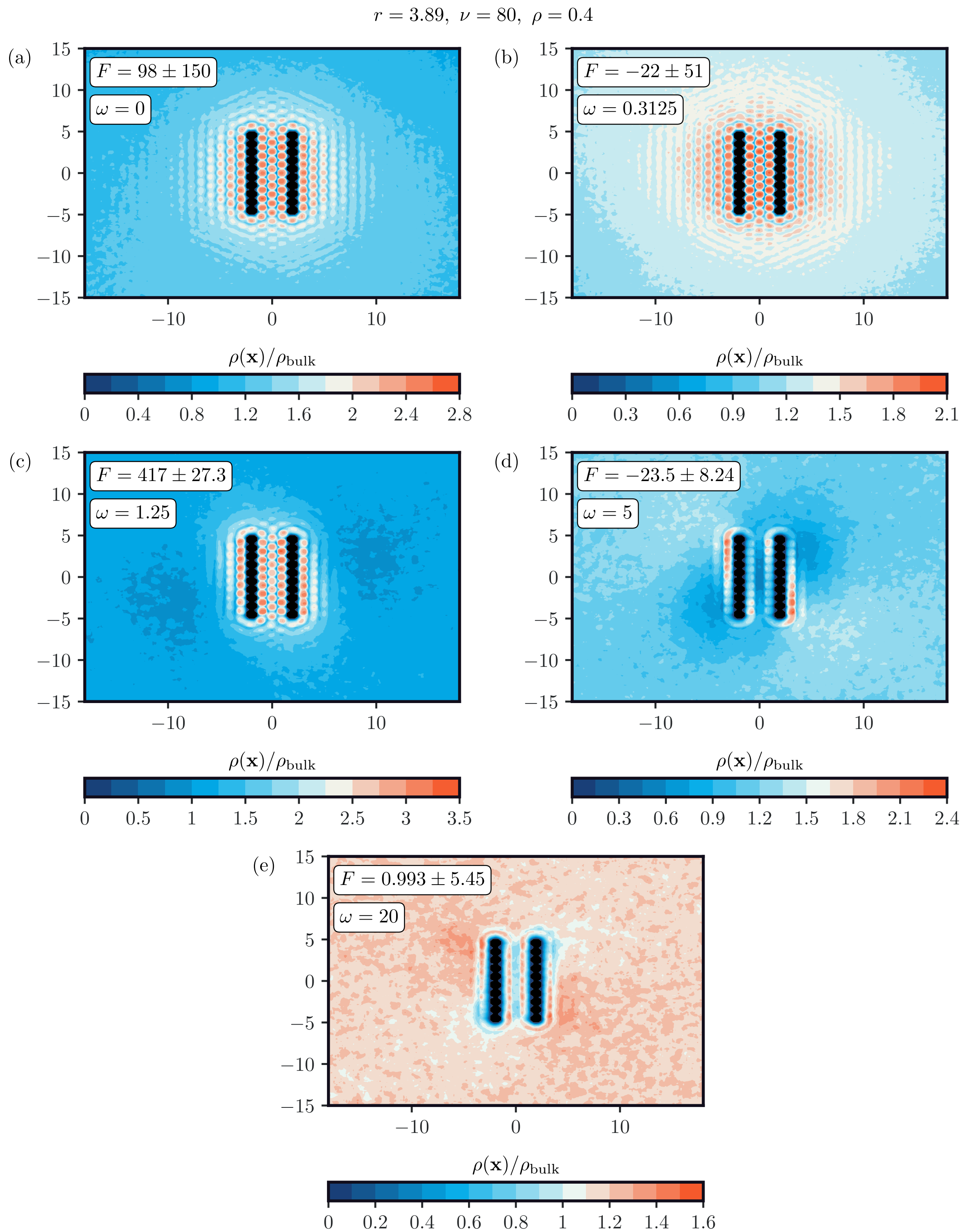

FIG. S17: Density fields for a separation with near zero force between two passive walls in a chiral active Brownian particle bath.

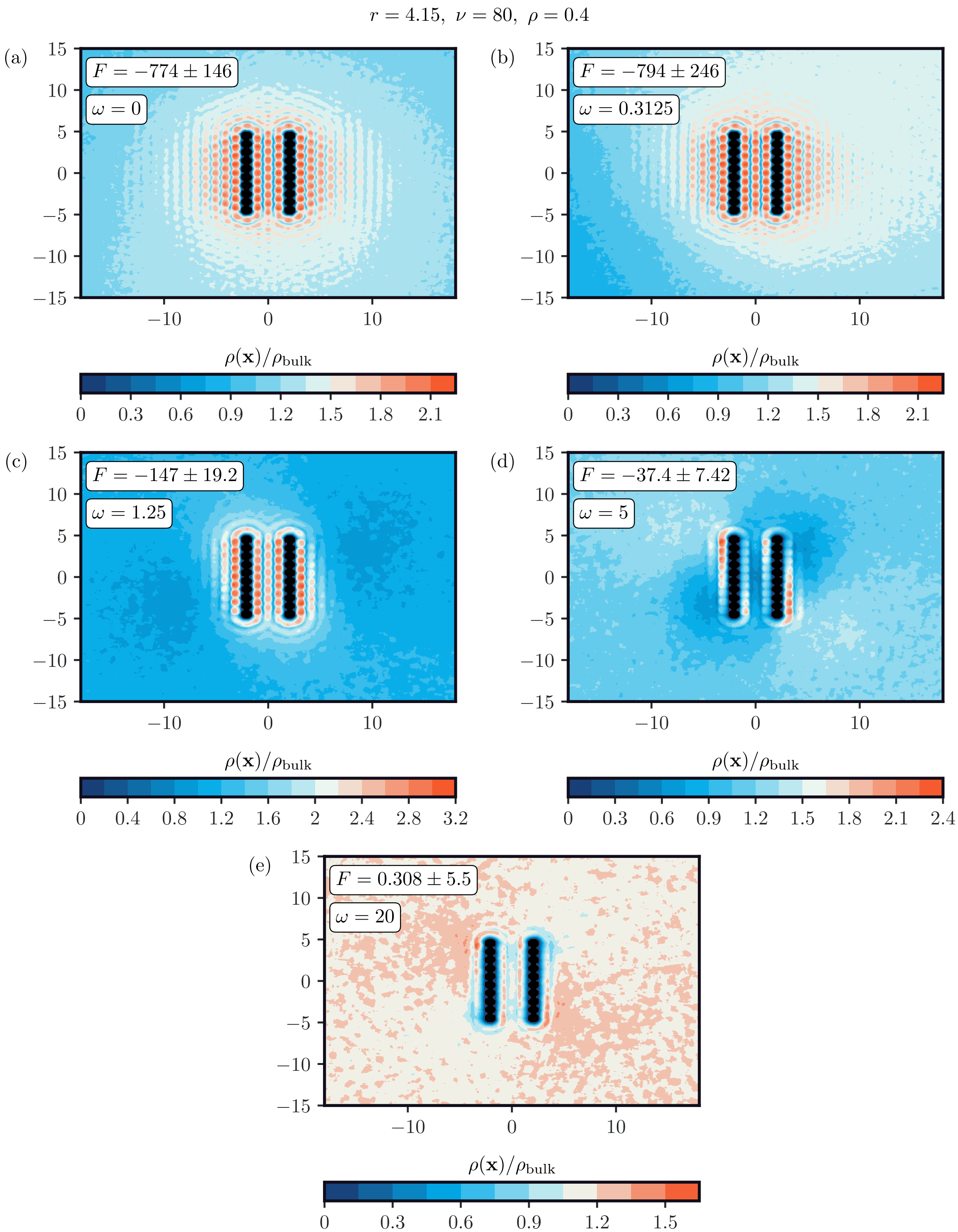

FIG. S18: Density fields for maximal attractive force between two passive walls in a chiral active Brownian particle bath.

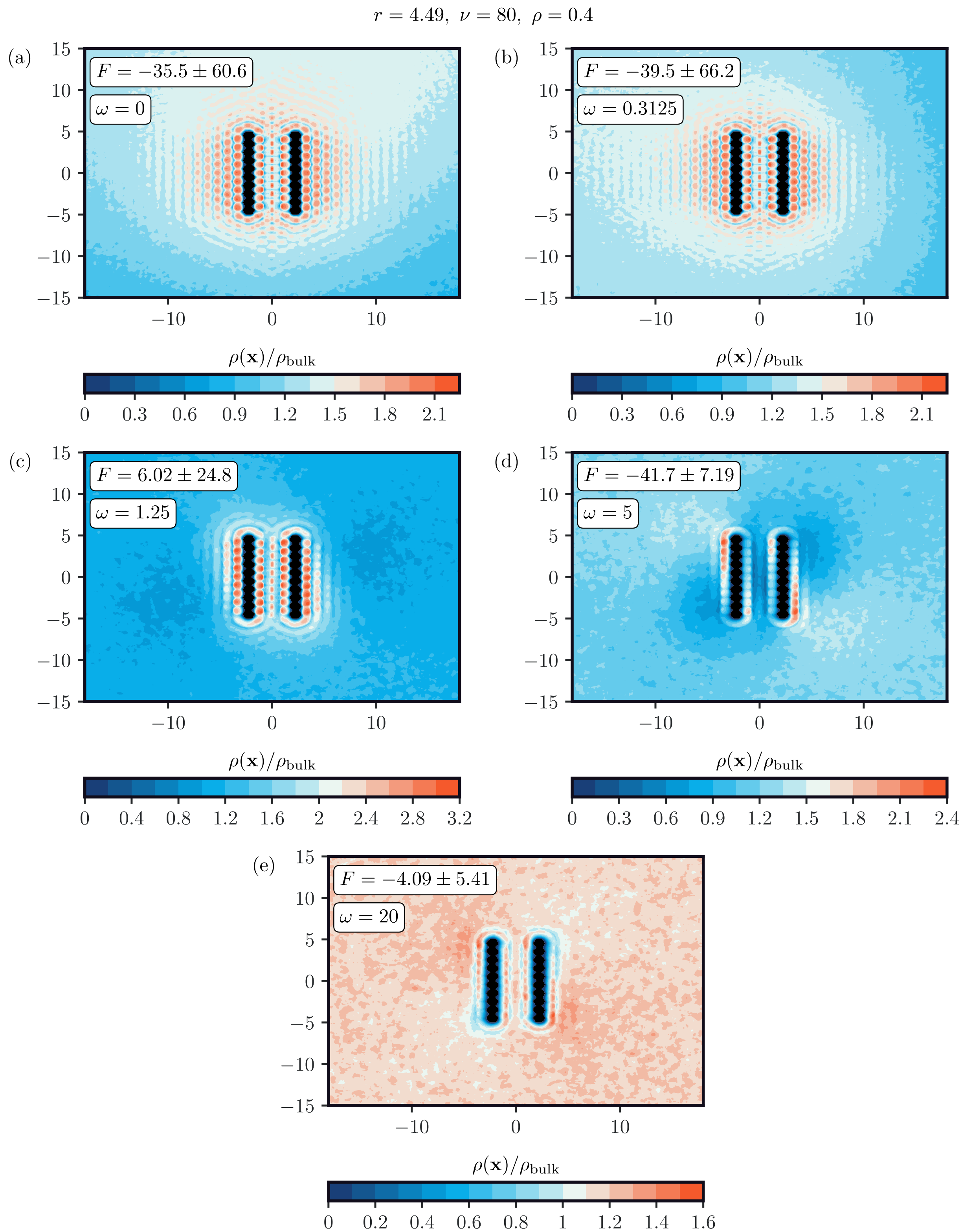

FIG. S19: Density fields for a separation with near zero force between two passive walls in a chiral active Brownian particle bath.

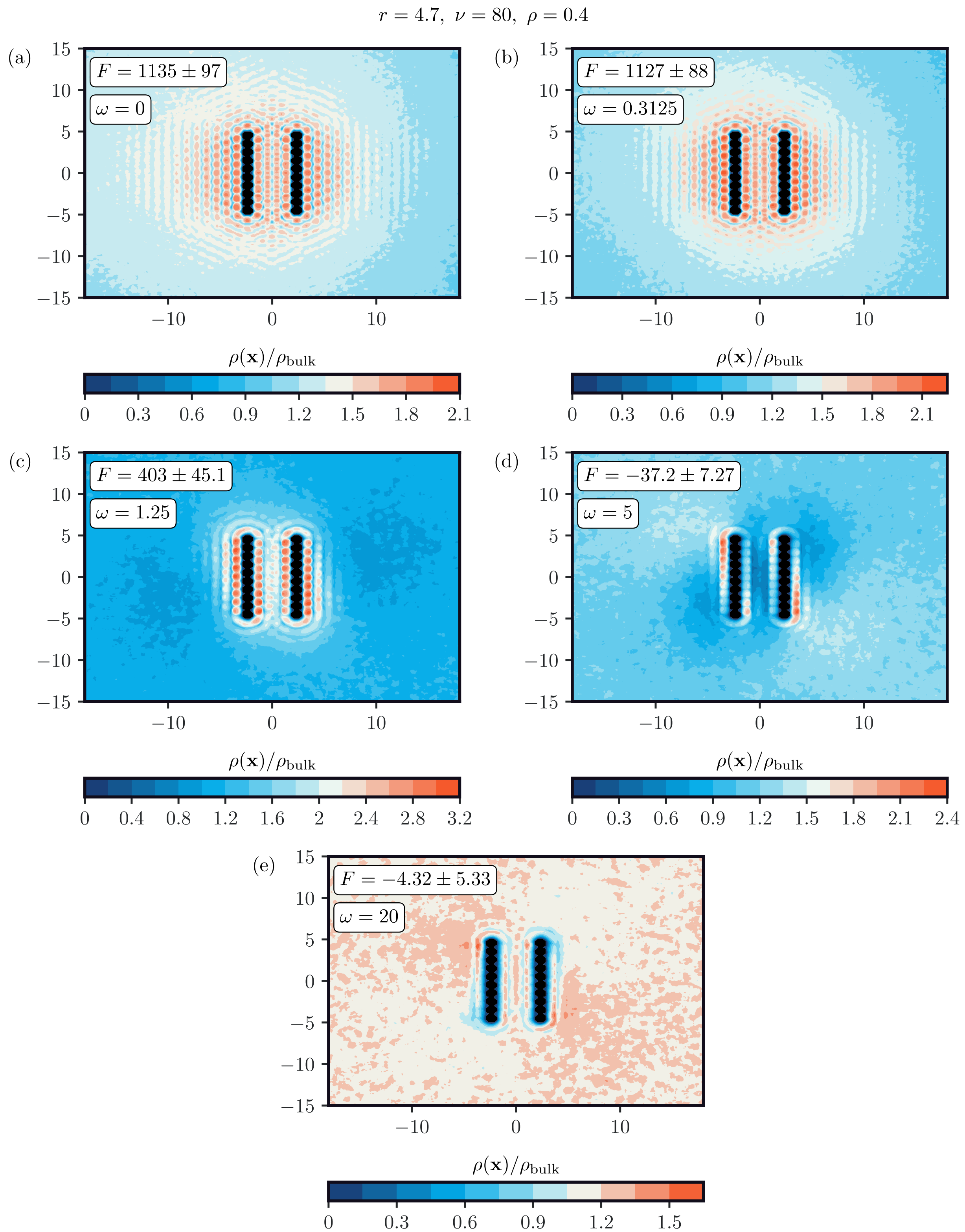

FIG. S20: Density fields for maximal repulsive force between two passive walls in a chiral active Brownian particle bath.

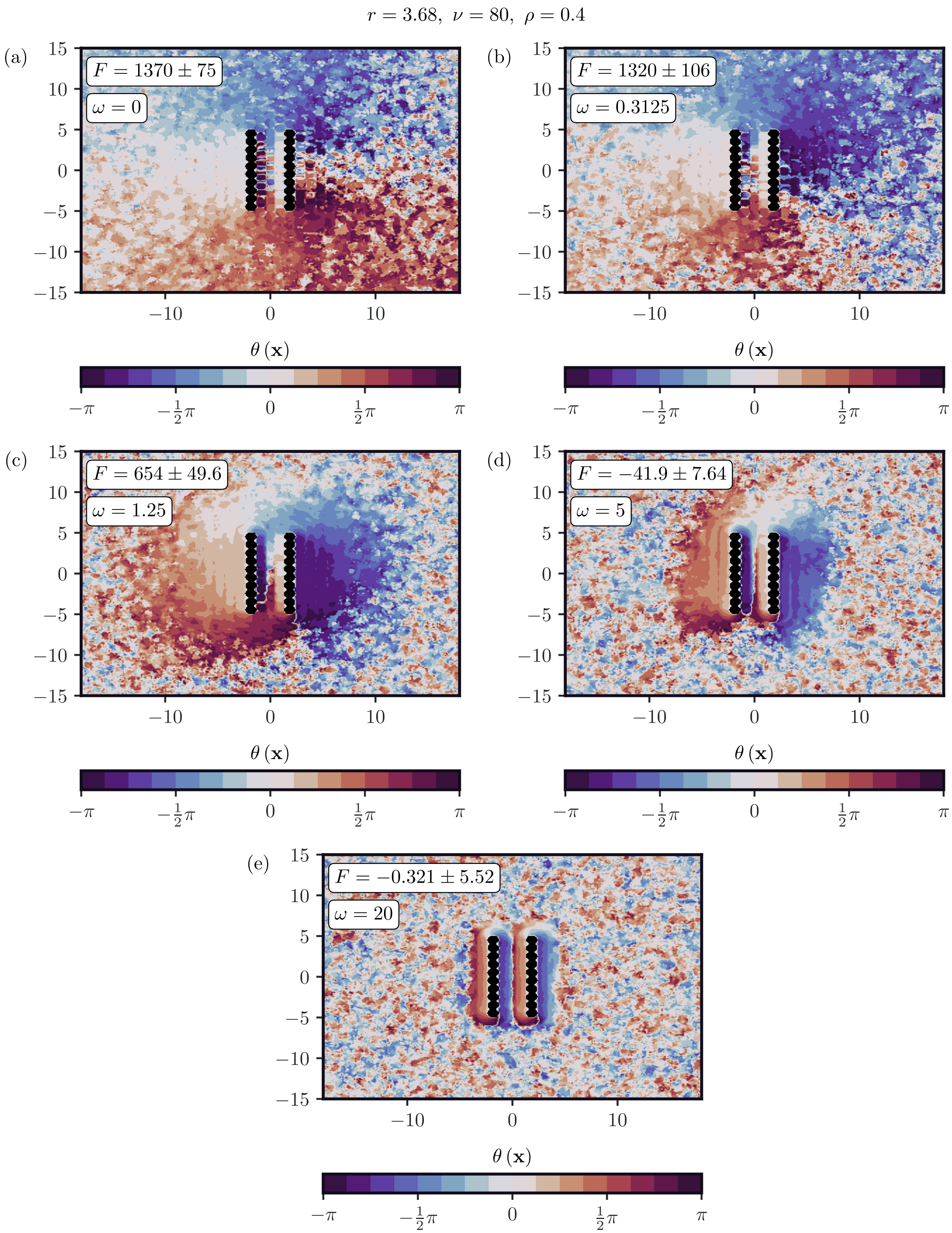

FIG. S21: Orientation fields for maximal repulsive force between two passive walls in a chiral active Brownian particle bath.

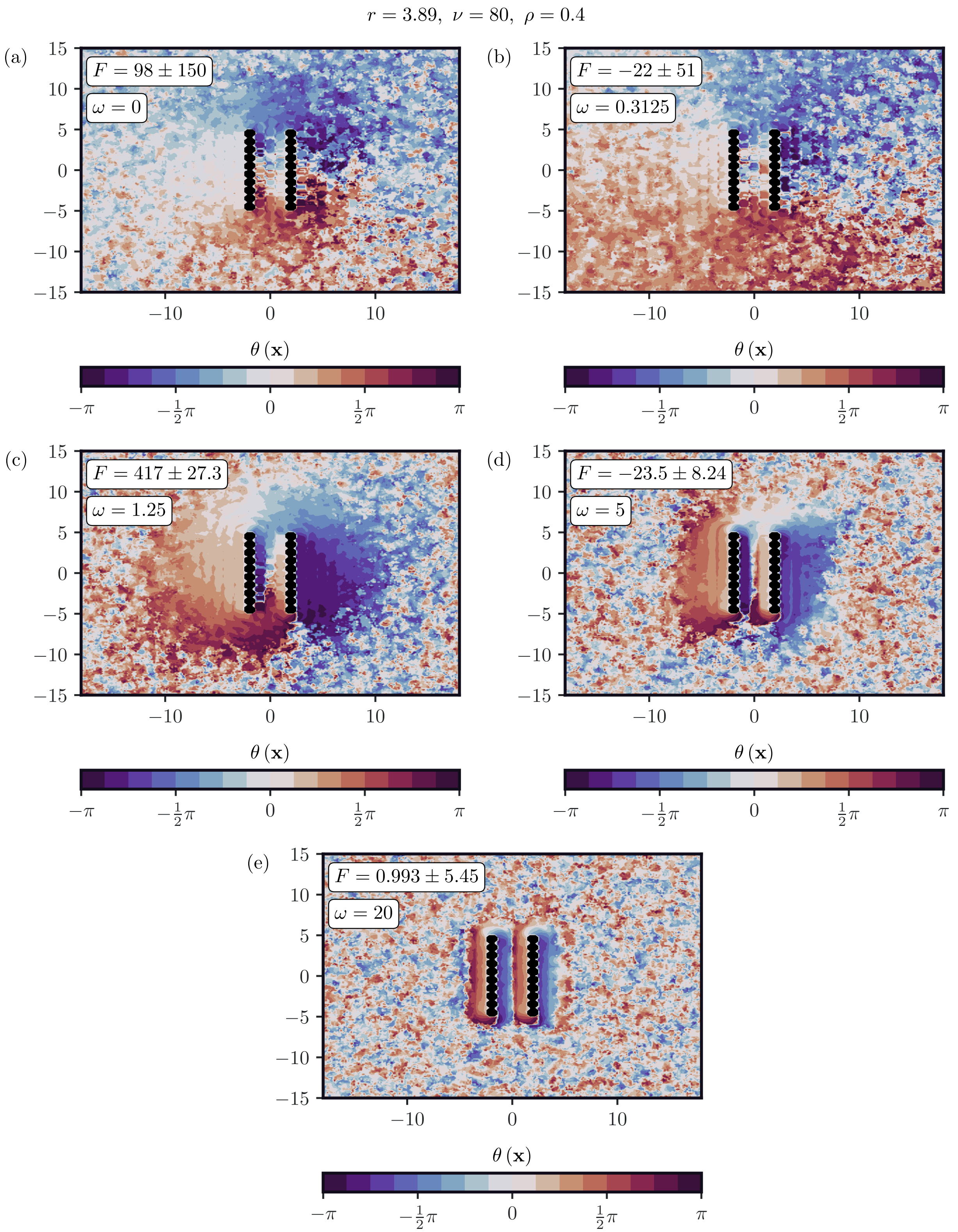

FIG. S22: Orientation fields for a separation with near zero force between two passive walls in a chiral active Brownian particle bath.

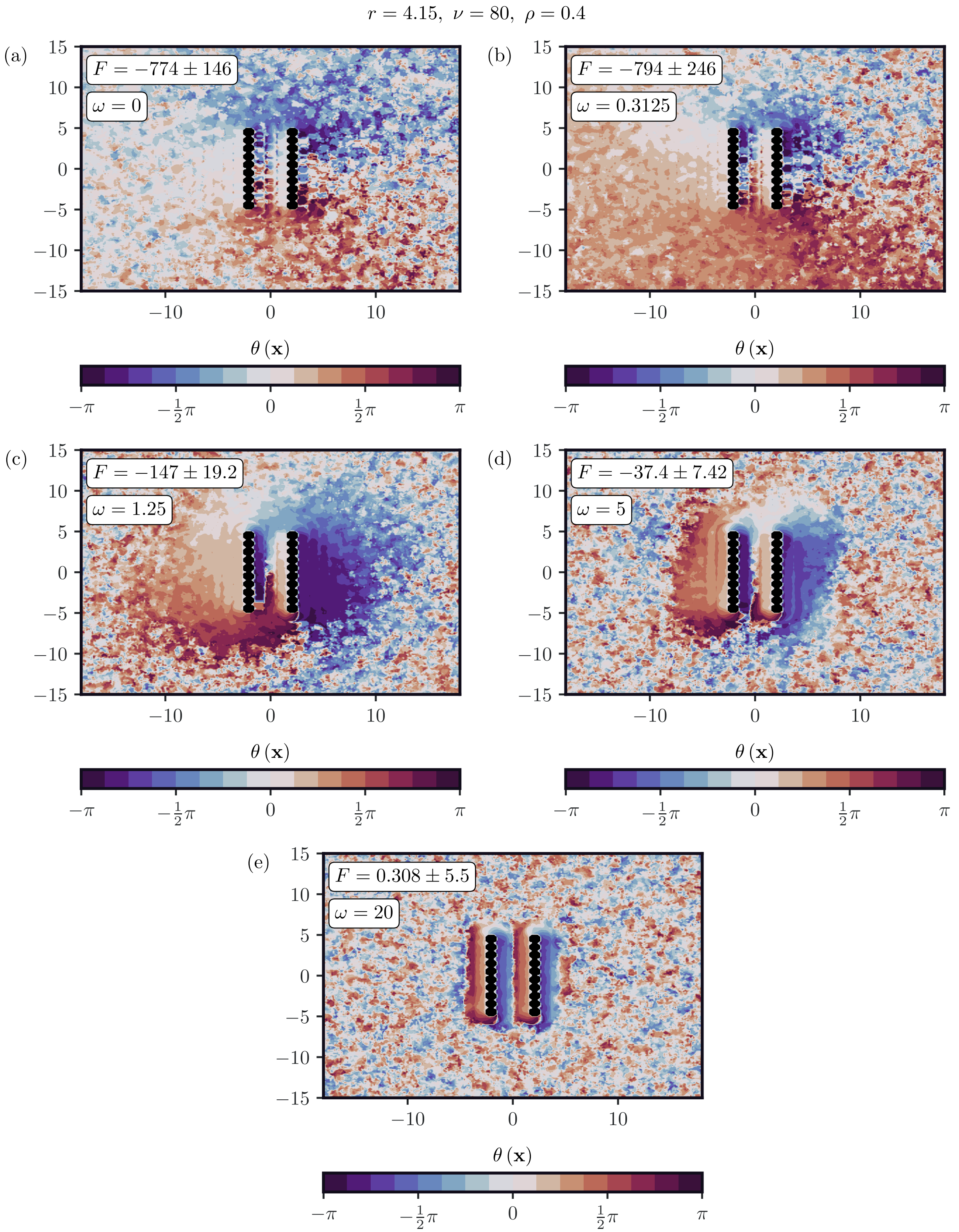

FIG. S23: Orientation fields for maximal attractive force between two passive walls in a chiral active Brownian particle bath.

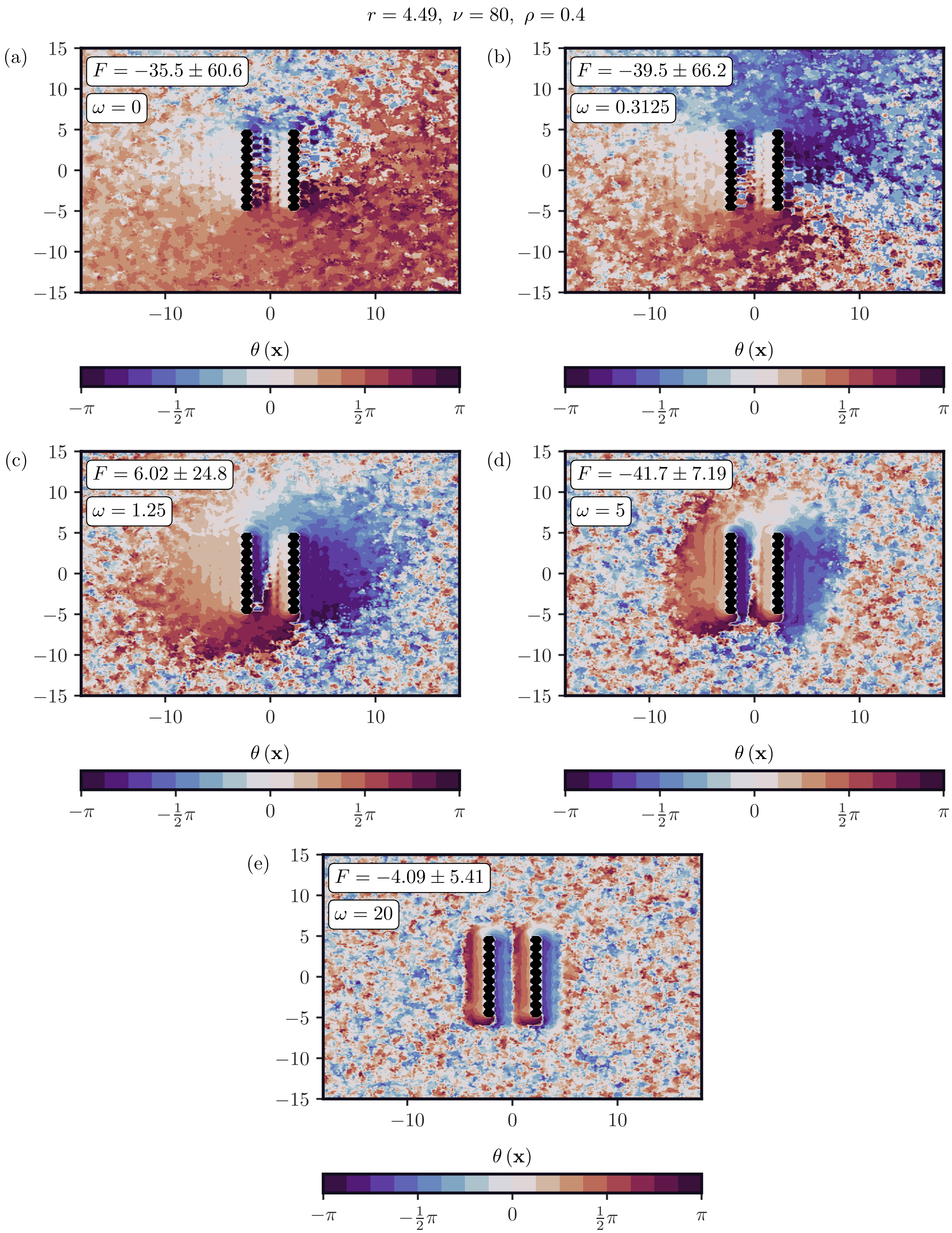

FIG. S24: Orientation fields for a separation with near zero force between two passive walls in a chiral active Brownian particle bath.

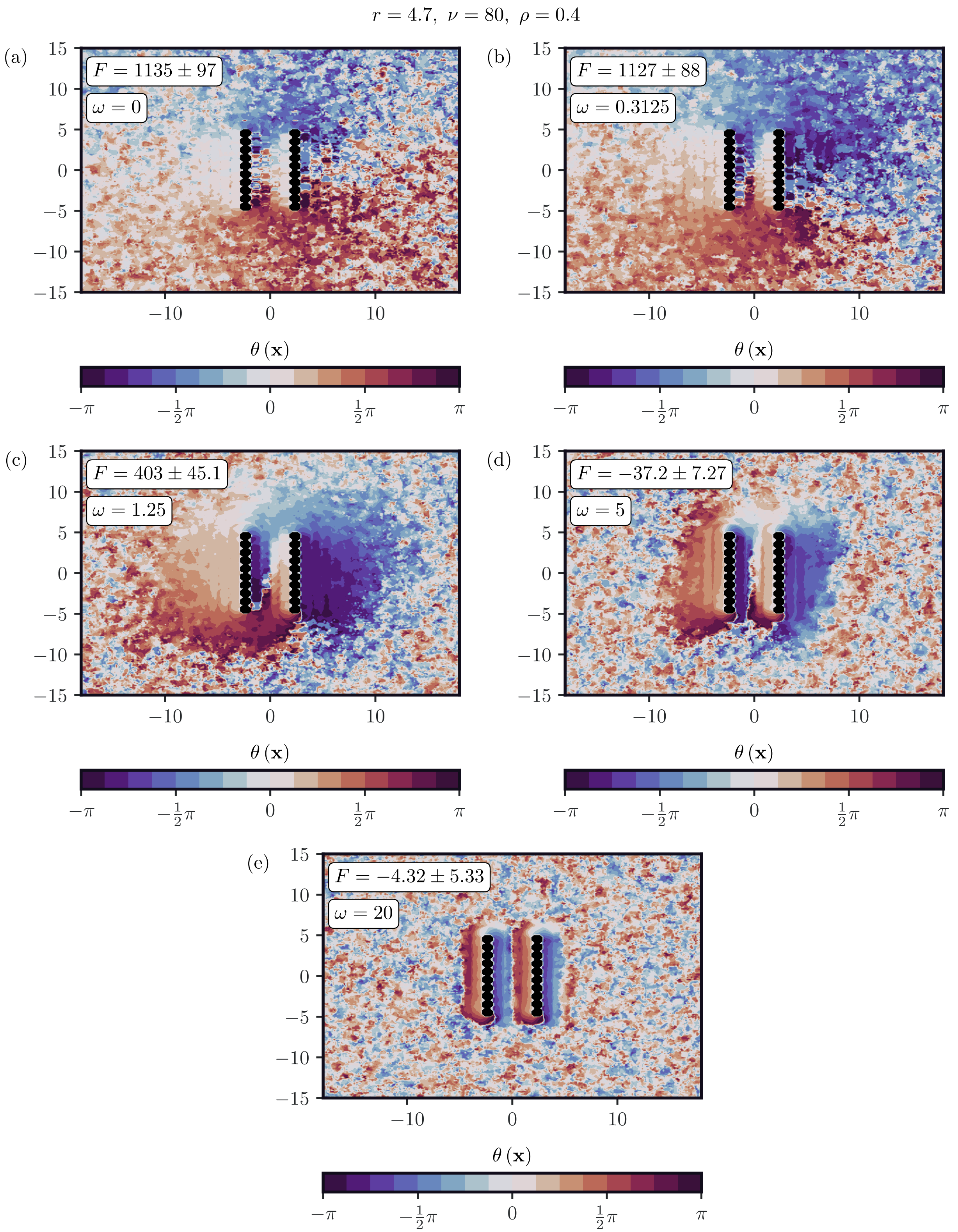

FIG. S25: Orientation fields for maximal repulsive force between two passive walls in a chiral active Brownian particle bath.